applied sciences

MDPI

Article

A Validated Thermal Computational Fluid Dynamics Model of Wine Warming in a Glass

Maximilian Kannapinn [1,*,†], Felix Köhler [2,†] and Michael Schäfer [2]

[1] Cyber-Physical Simulation, Department of Mechanical Engineering, Technical University of Darmstadt, Dolivostr. 15, 64293 Darmstadt, Germany
[2] Department of Mechanical Engineering, Institute for Numerical Methods in Mechanical Engineering, Technical University of Darmstadt, Dolivostr. 15, 64293 Darmstadt, Germany; koehler@fnb.tu-darmstadt.de (F.K.)
* Correspondence: kannapinn@cps.tu-darmstadt.de
† These authors contributed equally to this work.

Abstract: Oenophiles are aware that the temperature at the time of drinking can profoundly shape wine's sensory attributes. Wine is usually served and drunk below room temperature but warms up after pouring due to heat exchange with warmer surroundings. This study investigates how quickly wine warms up in a wine glass and identifies the relevant heating effects. A numerical simulation using conjugate heat transfer is established, representing the complex multi-physical process. Experiments are conducted to validate the simulation. It is shown that the simulation must take into account thermal conduction, convection, and even radiation to provide accurate results. Without simulating radiation and convection of the room air, the predicted temperature is off by 66.3% or 3.3 °C. As warming is independent of the alcohol content, the simulation results are valid for non-sparkling wine types with moderate sugar levels within the considered configuration. A parameter study investigated the temperature increase over time depending on the ambient temperature and the initial wine temperature for 150 mL wine in a medium-sized red wine glass. The results can provide information on preparing a wine to obtain the desired drinking temperature.

Keywords: wine; glass; conjugate heat transfer; simulation; CFD; thermal radiation

Citation: Kannapinn, M.; Köhler, F.; Schäfer, M. A Validated Thermal Computational Fluid Dynamics Model of Wine Warming in a Glass. *Appl. Sci.* **2024**, *14*, 8997. https://doi.org/10.3390/app14198997

Academic Editors: Francesco Duronio and Angelo De Vita

Received: 28 August 2024
Revised: 16 September 2024
Accepted: 26 September 2024
Published: 6 October 2024

1. Introduction

The drinking temperature significantly influences the perception of wine, as it affects the sensory attributes such as smell, taste, and mouthfeel [1]. Each wine type is usually most appreciated at an individual temperature according to its sensory characteristics. White wines are consumed relatively cool, whereas red wines are usually enjoyed slightly warmer but still below common room temperature [2]. In general, wine should be tempered appropriately before serving and drinking to provide the best taste experience. However, wine is often not drunk immediately after pouring and warms up in the glass due to thermal interaction with warmer surroundings. This should be considered when preparing wine. It is usually unknown how quickly the wine warms up in a glass. To the authors' knowledge, the warming of wine has not been the subject of a scientific investigation to date.

Literature on wine in the context of heat transfer and corresponding numerical simulation is scarce. Beamont et al. [3] investigated the bubble-driven flow of champagne in a glass with computational fluid dynamics (CFD). The group also conducted simulations with different, but fixed champagne temperatures for the same flow [4]. Other studies investigate the flow and thermodynamical processes in wine fermentation tanks with CFD methods [5–7]. Simulations were also used to examine the cooling and ventilation system of wine refrigerators [8,9] and wine cellars [10]. The rheological and thermodynamical properties of wine were investigated in some studies, e.g., [11–13].

Several studies showed the influence of the drinking temperature on the sensory attributes of wine. Cool temperatures decrease the human perception of sweetness and increase the perception of sourness [14]. Bitterness and astringency get more pronounced with decreasing wine temperature [14,15]. Higher wine temperatures increase volatility, allowing more compounds to dissolve from the wine in the glass and enhance the wine's aroma [1,15,16]. The panelists in a study by Ross et al. [16] perceived red wines at 16 °C rather as bitter and astringent and less sweet compared to the same wines tasted at 22 °C. The red wines were more often described with aromatic attributes at 16 °C than at 10 °C. According to [2,17], wine can smell and taste too alcoholic when it is too warm due to the accelerated evaporation of ethanol.

Although the drinking temperature preference may be individual, there are general guidelines for the serving temperature of the different wine types. The Oxford companion on wine by Robinson and Harding [2] specifies that full or tannic red wines should be served at 15 °C to 18 °C. In contrast, medium-bodied and light red wines are usually offered a few degrees colder. Full and complex dry white wines should be served at 12 °C to 16 °C. Dry (aromatic) white wines with a medium or light body are liked most at around 8 °C to 12 °C serving temperature. Sweet, light white wines should be offered even cooler at around 5 °C to 10 °C. It is recommended that the wine should usually be served at the lower end of the indicated ranges since it warms up relatively fast in the glass [2]. To the best of the authors' knowledge, no profound information is available on how fast wine warms up in a glass.

This study aims to close this gap and examines the physical process of wine warming in a glass and determines the wine's temperature change over time. The warming process is modeled and computed using numerical simulation. The simulation can reveal the governing heating phenomena and can be easily applied to different configurations for similar heating problems. A conjugate heat transfer simulation models the crucial heating mechanisms such as thermal conduction, convection, and radiation. The simulation approach considers only non-sparkling wines. Buoyancy effects due to rising bubbles are not included. Sweet dessert wines or fortified wines with high sugar content are not examined either. The study focuses on one configuration with one specific glass and filling quantity to closely investigate the physical process and the applied computational methods. Experiments are presented providing reference data to evaluate and validate the simulation approach. The importance of modeling the different heating mechanisms is examined in detail.

The temperature increase of wine is determined for various combinations of the initial wine temperature after pouring and ambient temperature. The results can inform sommeliers, restaurateurs, and wine enthusiasts about how wines should be tempered to reach the optimal drinking temperature under different room and storage conditions. For example, one could determine how long a red wine has to remain in a glass to reach a certain temperature when the bottle was stored cool at a known temperature. Red wine could also be stored at a specific low temperature to let it breathe in a glass for a given period while reaching the ideal drinking temperature. To optimize the drinking experience, especially on hot summer days, bars or restaurants could adjust the storage temperature of white wines based on ambient temperature and the time it takes to serve them. Besides practical advice, this study also gives insights into the physical effects of wine warming as the local and temporal influence of different heating mechanisms are investigated. The presented simulation approach could be utilized to develop new wine glasses with regard to their thermal behavior. Thus, producers could optimize the glass shape to potentially reduce wine warming.

The investigated configuration of wine warming in a glass is specified in Section 2. Experiments were conducted for the same configuration. The experimental setup, procedure, and results are presented in Section 2.1 and the following sections. Section 3 outlines the conjugate heat transfer simulation approach, including the governing equations, the material modeling and properties and the simulation setup. The simulation approach is validated with the experimental data in Section 4. Furthermore, the influence of different heating mechanisms and fluid properties is investigated. Section 5 presents the main results

and findings. The warming process is analyzed, and a parameter study for different initial and surrounding temperatures is performed. Section 6 summarizes the results and gives an outlook on potential further research questions.

2. Problem Configuration and Experiments

The study investigated the warming of 150 mL of non-sparkling wine in a medium-sized red wine glass. Figure 1b shows the glass dimensions of the CAD (computer-aided design) model that was derived from available drawings and measurements. The glass has a maximum outer diameter of 90 mm and a height of 225 mm. Its total capacity is 490 mL. With the coordinate system originating in the bottom of the glass's center, the wine surface is located at $y_{\text{surf}} = 142$ mm. The glass's dimensions are similar to universal wine glasses used for white and red wine. The glass is only slightly larger than many white wine glasses. Therefore, it could also be used to consume white wine. The authors purchased the glass from the producer Stölzle Lausitz GmbH (Weißwasser/Oberlausitz, Germany).

(**a**) (**b**)

Figure 1. Experimental setup and CAD model of a wine glass with 150 mL of wine. (**a**) Experimental setup with a Greisinger thermometer (Regenstauf, Germany), the PT 1000 sensor is positioned in the center of the wine glass. (**b**) CAD model (dimensions in mm).

The filled glass was positioned on a wooden table in an empty room. Table, air, and room walls were initially at the same temperature, referred to as the room temperature T_{R}. The initial wine temperature T_0 was less than T_{R}. The configuration did not experience external influences like hands touching the glass or swirling. The effect of the pouring process was neglected. Thus, the wine warmed up only through heat exchange with the warmer surroundings.

2.1. Experimental Setup and Procedure

The experimental study investigated the warming of red wine, white wine, and tap water at $T_{\text{R}} = 23\,^{\circ}\text{C}$. Two experiments were performed according to the configuration described above to obtain comprehensive reference data for validation. In the first experiment, the average temperature of wine and water was measured after predefined periods. The second one determined the temperature increase over time of water at specified locations inside the glass. The experiments included tap water to simplify the comparability to the simulation for detailed validation and to investigate the liquid composition's influence.

Figure 1a shows the experimental setup. A Greisinger resistance thermometer with a platinum sensor (Pt1000, accuracy $\pm 0.1\,^{\circ}\text{C}$ for $T \in [-20\,, 150\,]\,^{\circ}\text{C}$) was used as in similar experiments related to food [18,19] and wine [20]. A mounting device fixed the thermometer sensor in a vertical direction above the glass. The sensor tip was positioned inside the liquid (wine or water) and could be moved in a vertical direction. The diameter of the cylindrical sensor was 1.5 mm. The mass of the sensor was relatively small compared to the mass of the wines, which allowed the assumption of negligible heat transfer from the thermometer to the liquid. The mounting device was designed to influence the physical

processes as little as possible. The glass was placed in the middle of a spruce wooden board, with the dimensions 800 × 400 × 18 mm. The examined red wine was from Primitivo grapes containing 13.5 % of volume alcohol, 10.7 g L^{-1} (grams per liter) residual sugar, and 6.8 g L^{-1} acidity. The white wine was a Cuvee with 11.5% of volume alcohol, 11.8 g L^{-1} residual sugar, and 6.5 g L^{-1} acidity, as communicated by the producers.

Before starting the experiments, the wine and tap water were kept cool in a refrigerator at 6 °C. 150 mL of the corresponding liquid were poured into a calibrated measuring cylinder, with an accuracy of ±2 mL. The liquid was slowly heated until it nearly reached the required initial temperature to account for the temperature increase during the pouring. The small temperature change was caused by interaction with the air and was about 0.2 °C for $T_0 = 12$ °C. The liquid was poured into the glass, where the thermometer sensor was placed to verify the correct initial temperature immediately after finishing the pouring process. The timing started as soon as the liquid had been poured into the glass.

2.2. Average Wine and Water Temperatures

For the first experiment, the thermometer sensor was removed from the glass immediately after pouring and measuring the initial liquid temperature. The experimental setup was not disturbed for 5, 10, 20, or 40 min, respectively. Afterwards, the liquid was mixed quickly in the glass with a plastic stirring device to achieve a uniform temperature distribution without introducing additional heat. The temperature was measured in the middle of the liquid. The result was taken as the average temperature of the water or wine in the glass.

This experiment was performed with red wine and water for the initial temperatures of 8 °C and 12 °C. The white wine was measured for $T_0 = 8$ °C. The experiment was conducted five times for each period and liquid. Figure 2a,b present the mean temperature and the standard deviation of the measurements. After each period, the mean temperature is nearly the same for water, red, and white wine. The maximal difference is only about 0.2 °C between the mean temperature of the water and red wine for $T_0 = 8$ °C after 40 min. The results indicate that, apart from water, the additional components in wine do not significantly affect the warming process in the glass. The impact of the alcohol content seems to be negligible, considering the difference of 13.5 % alcohol between red wine and water. Furthermore, there is no notable difference between the red wine and white wine with 11.5 % alcohol in terms of warming at similar sugar and acidity levels. The investigated wines contain a moderate sugar content, typical of semi-dry wines [2]. Sugar is the only component that can vastly vary between dry and sweet wines, in quantity, relevant to the warming [21]. Therefore, the warming process could differ for wines with a significantly higher sugar content, which is not explored here. The standard deviations are relatively small. Hence, only the mean temperatures are included in the figures throughout this work.

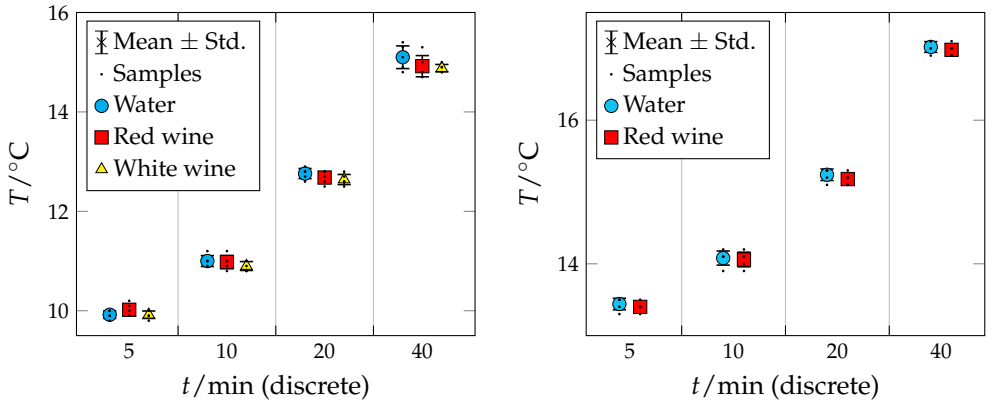

(**a**) $T_0 = 8$ °C. (**b**) $T_0 = 12$ °C.

Figure 2. Average wine and water temperatures after specified warming periods at room temperature $T_R = 23$ °C.

2.3. Temperature Increase of Water over Time

The second experiment determined the temperature of water with $T_0 = 12\,^{\circ}\mathrm{C}$ over time at three positions along the glass symmetry axis. The temperature was measured in the center of the glass ($x = 0\,\mathrm{mm}$) at 10, 20 and 30 mm below the water surface. The corresponding positions are denoted y_1, y_2, and y_3, i.e., $y_1 = y_{\mathrm{surf}} - 10\,\mathrm{mm}$. It should be noted that the thermometer sensor tip was located 2 mm below the specified positions since the temperature is measured over a small distance and not directly at the end. The sensor stayed in the water for 45 min while the experimental setup was not disturbed. The temperature was measured and recorded every five seconds. The measurement over the entire period was conducted five times for each position. The mean of the five measurements in each time stamp and the corresponding standard deviation are shown in Figure 3. The standard deviation decreases with the increasing distance from the water surface, but it is still reasonably small at y_1. The layered results from y_1 to y_3 suggest a stratification of temperatures within the wine. The numerical investigations will reveal why natural convection effects cannot diminish the stratification.

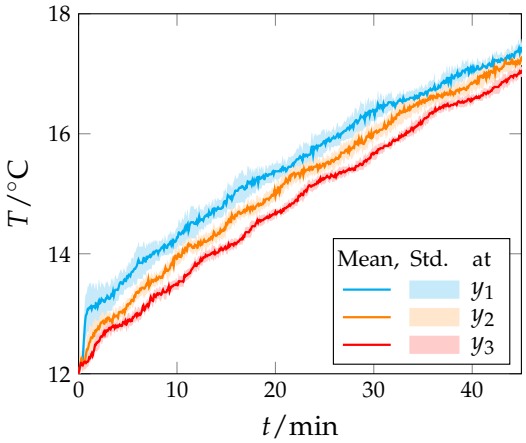

Figure 3. Temperature increase of water over time at 10, 20, and 30 mm below the water surface in the glass center (denoted y_1, y_2, and y_3) at $T_{\mathrm{R}} = 23\,^{\circ}\mathrm{C}$.

3. Simulation Model

The simulation approach applied a three-dimensional model to represent the investigated problem configuration, as described in Section 2. The model considers the wine, glass, surrounding air, and table. A conjugate heat transfer simulation models the crucial heating mechanisms (such as thermal conduction, convection, and radiation). The physical quantities are determined in space and time by numerically solving the governing equations for the problem domain. The simulated wine corresponds to the previously presented red wine. The white wine was not assessed as the experiments indicated no difference in the warming process between red and white wine. The material properties used to model the fluids and solids, the governing equations, and computational methods are presented in the following.

3.1. Conjugate Heat Transfer

Describing the non-isothermal flow of air and wine involves conserving mass, momentum, and energy. The differential form of the Navier–Stokes equations reads

$$\frac{\partial \rho}{\partial t} + \frac{\partial (\rho v_i)}{\partial x_i} = 0\,, \tag{1}$$

$$\frac{\partial (\rho v_i)}{\partial t} + \frac{\partial (\rho v_i v_j)}{\partial x_j} = -\frac{\partial p}{\partial x_i} + \frac{\partial \tau_{ij}}{\partial x_j} + \rho g_i\,, \tag{2}$$

$$\frac{\partial (\rho h)}{\partial t} + \frac{\partial (\rho h v_i)}{\partial x_i} = \frac{\partial p}{\partial t} + \frac{\partial (\tau_{ij} v_j)}{\partial x_i} + \rho g_i v_i - \frac{\partial q_i^{\mathrm{S}}}{\partial x_i}\,, \tag{3}$$

where t is time, x_i are cartesian coordinates, v_i are fluid velocities, ρ represents density, p is pressure, h is total enthalpy, and g_i is the gravitational acceleration vector. For surface heat fluxes q_i^{S}, Fourier's law in isotropic configuration,

$$q_i^{\mathrm{S}} = -\kappa \frac{\partial T}{\partial x_i} \tag{4}$$

is applied, where κ represents the thermal conductivity and T is temperature. The viscous stress tensor τ_{ij} of a Newtonian fluid reads

$$\tau_{ij} = \mu \left(\frac{\partial v_i}{\partial x_j} + \frac{\partial v_j}{\partial x_i} \right) - \frac{2}{3} \mu \frac{\partial v_k}{\partial x_k} \delta_{ij}\,, \tag{5}$$

where μ represents dynamic viscosity and δ_{ij} is the Kronecker delta. In Equation (3), viscous heating $\frac{\partial}{\partial x_i}(\tau_{ij} v_j)$ can be omitted for flows without enormous velocity gradients [22], and work by gravitational forces $\rho g_i v_i$ are neglected by the solver [23]. The gravitational body force ρg_i remains included, as buoyant effects are expected to dominate. All fluid flows are assumed to remain in the laminar regime. In addition to the constitutive material law for the fluid, compared to Equation (5), the thermal and caloric equations of state for density $\rho = \rho(p, T)$ and specific heat capacity $c_p = c_p(p, T)$ close the system of equations describing non-isothermal fluid flow. Boundary conditions and material properties for the given problem are presented in the following sections. For conjugate heat transfer simulations in solids, the total enthalpy equation (Equation (3)) can be simplified with $v_i = 0$ and $\mathrm{d}p = 0$ to

$$\frac{\partial (\rho h)}{\partial t} = \frac{\partial}{\partial x_i} \left(\kappa \frac{\partial T}{\partial x_i} \right). \tag{6}$$

Thermal radiation within the space around the glass represents the third mode of heat transfer besides convection and conduction. In the limit case of a non-participating medium, the net radiative heat transfer between surfaces $q_{\mathrm{rad,net}}$ can be included in the boundary condition for Equation (3). It can be derived from the radiative energy conservation at the surface k of a gray body. Let G_k be the incoming radiative heat flux, also called the irradiation. The radiosity J_k, the total radiative heat flux leaving the surface, is

$$J_k = \epsilon_k E_{\mathrm{b},k} + \mathcal{R}_k G_k\,, \tag{7}$$

where $E_{\mathrm{b},k} = \sigma T^4$ is the black body emissive power, ϵ_k is the emissivity, and $\mathcal{R}_k$ is the fraction of irradiation diffusely reflected by the surface. Taking the difference between radiosity and irradiation yields the net outgoing radiative heat flux

$$q_{k,\mathrm{rad,net}} = J_k - G_k = \epsilon_k E_{\mathrm{b},k} + \mathcal{R}_k G_k - G_k\,. \tag{8}$$

Obeying the energy balance for opaque surfaces, $\mathcal{A}_k + \mathcal{R}_k = 1$, where $\mathcal{A}_k$ is the body's absorptivity, and applying Kirchoff's law for gray bodies ($\mathcal{A}_k = \epsilon_k$) [24] yields

$$q_{k,\mathrm{rad,net}} = \epsilon_k E_{\mathrm{b},k} - \mathcal{A}_k G_k = \epsilon_k (E_{\mathrm{b},k} - G_k) \tag{9}$$

for the additional radiative heat fluxes in the boundary condition for Equation (3). Equation (9) requires G_k, the irradiation of all other surfaces that engage in the radiative heat exchange. Shah [25] developed the discrete transfer radiation model to solve the radiative transfer equation for the intensity $I(s)$ in discrete directions s emanating from the boundary surfaces with normal vectors n. A fixed number of rays are emitted in the hemisphere's discrete polar and azimuthal angles. In the absence of an attenuating fluid, the total irradiation of one surface is given by the integral

$$G_k = \int_{s \cdot n > 0} I(s)\, s \cdot n \, \mathrm{d}\Omega \tag{10}$$

over all hemispherical solid angles Ω [23].

3.2. Material Properties

The wine is modeled as an aqueous ethanol solution. Further compounds make up a much smaller proportion of the wine than ethanol and are, therefore, neglected [21]. The amount of sugar and acid in the investigated red wine is more than ten times lower compared to ethanol. Some sweet wines could probably contain a non-negligible amount of sugar but are not considered here; see discussion in Section 1. Ethanol's volume fraction $\phi_{\mathrm{eth}} = 13.5\%$ of the utilized red wine equals a mass fraction of $\omega_{\mathrm{eth}} = 0.1086$. Melinder [26] provides temperature-dependent transport properties of an aqueous ethanol solution with $\omega_{\mathrm{eth}} = 0.1$, see Table 1, which were used for all simulations of red wine hereafter. Temperature-dependent transport properties of water were taken from [27]. While the visible solar radiation gets transmitted through water, low-frequency radiation ($\lambda > 0.95\,\mu\mathrm{m}$) is absorbed within a layer of approximately 2 mm [28]. Consequently, the liquid surface is treated as opaque for thermal radiation, having an emissivity of $\epsilon_{\mathrm{liq}} = 0.96$ [29].

Table 1. Transport properties of a $\omega_{\mathrm{eth}} = 0.1$ aqueous ethanol solution [26].

T/°C	ρ/kg m^{-3}	c_p/J kg^{-1} K^{-1}	κ/W m^{-1} K^{-1}	μ/Pa s
0	984.9	4360	0.503	0.00325
10	983.8	4310	0.516	0.00217
20	982.0	4280	0.529	0.00153
30	978.7	4270	0.542	0.00116

The surrounding room air is considered an ideal gas with a variable density of $\rho_{\mathrm{air}} = \frac{pM}{RT}$, where M is the molecular weight of air, and R is the universal gas constant. The residual temperature-dependent transport coefficients of dry air ($c_{\mathrm{p}}, \kappa, \mu$) are taken from [27]. The influence of humidity on the transport properties can be neglected for the considered temperature range, see [30] for a comparison of dry and humid air. Air is considered an optically thin medium in this study. Only CO_2 and H_2O interact significantly with thermal radiation [28]. Those air components exhibit relatively low partial pressures at room temperatures under standard atmospheric pressures and low relative humidity. Consequently, their contribution to radiative heat transfer can be neglected.

Transport properties of the glass and the table were not easily found in a single, coherent and, hence, had to be combined from various sources; see Table 2. The thermal radiation of the surrounding white walls ($\epsilon_{\mathrm{wall}} \approx 1$) lies in the infrared band. While the visible solar radiation gets transmitted through glass, it absorbs a large share of infrared radiation [28]. This legitimates the modeling of glass as an opaque body ($\epsilon_{\mathrm{glass}} = 0.84$ for soda-lime glass) within this study.

Table 2. Transport properties of solids. Material data are kindly provided by Stölzle Lausitz GmbH if not marked otherwise.

Solid	ρ/kg m^{-3}	c_p/J kg^{-1} K^{-1}	κ/W m^{-1} K^{-1}	ϵ/—
Glass	2640	850	1.12	0.84 [31]
Spruce	430 [27]	2300 [32]	0.11 [33]	0.89 [34]

3.3. Computational Methods

The problem was implemented in ANSYS CFX 2021R1, a commercial CFD solver applying the finite volume method with a second-order spatial and temporal discretization. It was assumed that all liquid domains exhibit incompressible flow, as no flows with a high Mach number ($Ma > 0.3$) occurred in the study. The temperature-dependent density was still taken into account in order to resolve the natural convection phenomena [23]. The surrounding room was modeled as a spherical dome with a diameter of 2 m over a circular virtual table of the same dimension; see Figure 4. Exploiting symmetry, only one-half of the model needed to be resolved computationally and symmetry conditions were imposed. Smaller sector models produced distorted mesh elements at the symmetry axis and, consequently, were not used. The following boundary conditions were assigned: On the half-sphere and the lower side of the table, the temperature was fixed to the room temperature T_R. All air and wine boundaries had no slip conditions for the fluid flow. At the interfaces air–table, air–glass, air–wine, wine–glass, and glass–table, the conjugate heat transfer capability of ANSYS CFX 2021R1. ensured the continuity of temperatures and heat fluxes. Symmetry conditions were applied on all boundaries in the cut plane of the half model. The half-sphere surface was modeled as a wall, and, as the utilized solver, was sensitive to pressure head differences in open-cavity natural convection scenarios. The default inclusion of hydro-static pressures in the buoyancy forces induced spurious flows for open domains, as demonstrated in [35]. Concerning initial conditions, the initial velocities and relative pressures of air, water, or wine were zero. Air, wine glass, table, and room walls are initialized with the room temperature T_R, while the fluid temperature was initially set to T_0.

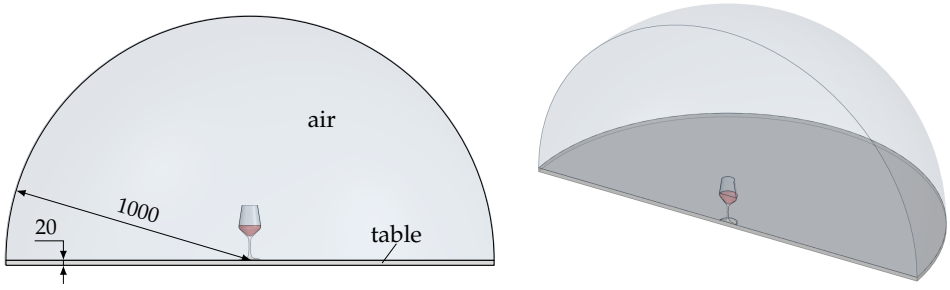

Figure 4. Computational domain of the half-model using symmetry boundary conditions in 2D view (**left**) and 3D view (**right**) (dimensions in mm).

The computational domain was discretized with hexahedral elements having a height of 2, 2, 0.5, and 1 mm for the domains table, air, glass, and wine, respectively. Figure 5 illustrates relevant sections of the final computational mesh. Inflation layers (15 and 11 layers for air and wine domain, stretch factor 1.2, and first layer height 0.1 mm) captured wall-bounded gradients in the domains of air and wine. Generalized Richardson extrapolation [36] was employed to estimate the grid-independent solution of the average heat fluxes at the domain interfaces. The relative discretization errors of 0.49 %, 1.04 %, and 0.29 % compared to the grid-independent solution were calculated for the domains air, glass, and wine. The resulting system was discretized into 492,042 control volumes. The initial 150 s were solved with a time step of 0.1 s, while the residual simulation utilized a time step of 0.5 s, as results did not differ significantly for smaller time steps. The system of equations was solved block-coupled for momentum and mass conservation and segregated for the

energy equation. The target scaled residuals of ANSYS CFX reached $R < 1 \times 10^{-6}$ for each time step, and imbalances were monitored to remain below 1 %. One simulation of 45 min real time took approximately 18 h on 16 cores of a cluster PC with two Intel Xeon E5-2687W v4 (3.2 GHz) CPUs (Santa Clara, CA, USA).

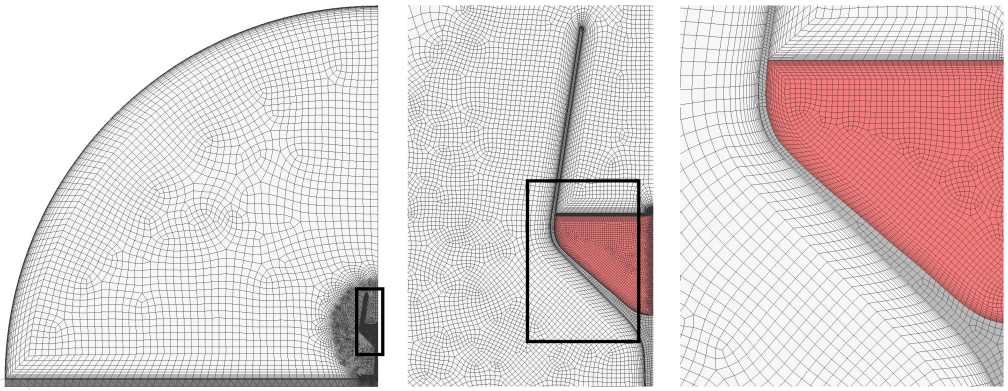

Figure 5. Quarter section of the discretized problem domain and two relevant close-ups.

4. Validation

The presented simulation approach was validated for warming wine and water at a room temperature of $T_R = 23\,°C$. The simulation results for the initial temperature of $T_0 = 8\,°C$ and $T_0 = 12\,°C$ were compared to the experimental data from Sections 2.2 and 2.3. Detailed validation was first performed for water rather than wine to reduce the possibility of modeling errors for the liquid. The following investigates the importance of modeling different physical heating mechanisms closely. Then, the simulation of wine was evaluated, and the effects of the liquid properties are discussed.

Figure 6 presents the results for warming water. The simulated temperature increase, see Figure 6a, and fits the experimental data accurately in all three positions. The temperature is computed slightly too low only for y_2. The initial rapid temperature increase starts with a delay of about 40 s. Minor differences in the initial conditions between the experiment and simulation are probably the reason for this. The pouring process in the experiment presumably introduces a small initial motion in the water so that the heat is transported faster from the glass wall to the middle of the liquid. The simulation takes a few seconds to establish the natural convection since starting from a zero velocity field. Nevertheless, the agreement is surprisingly accurate, considering the comparison in single discrete positions of the underlying complex physical system.

Figure 6b compares the average water temperatures. The simulation matches the experimental data for all investigated periods well. The simulated temperature is slightly overpredicted for $T_0 = 12\,°C$. However, the difference is only 0.08 °C after 5 min and 0.09 °C after 40 min. This corresponds to a relative error of 5.5% and 1.8% in relation to the corresponding temperature change, respectively. It should be noted that the discrepancy is within the range of the thermometer's measurement accuracy. The comparison for $T_0 = 8\,°C$ shows slightly larger errors for $t = 5\,min$ and $t = 20\,min$. This could be due to the relatively small number of measurements, and the experiment's higher error sensitivity at lower temperatures. At $t = 20\,min$, the maximum difference is still relatively small with 4.4% or 0.21 °C, while the prediction for $t = 10\,min$ and $t = 40\,min$ is accurate. Overall, the simulation agrees very well with the experimental data and accurately represents the physical process of water warming in a glass.

The importance of including the physical effects of convection and radiation in the simulation is investigated hereafter. The influence of modeling both mechanisms on the total heat transfer is examined for the warming of water with $T_0 = 12\,°C$. The convection of the air and the liquid in the glass are involved in the physical process. The simulation approach can disregard the convection of the liquid and the air by not calculating the

corresponding velocity field. A simulation without radiation neglects Equation (9). All simulation variations still model heat conduction. The comprehensive baseline simulation, including all physical phenomena, is compared to the simulation without taking into account (1) the convection of the air, (2) the convection of the water, (3) the radiation, and (4) the radiation and convection of the air.

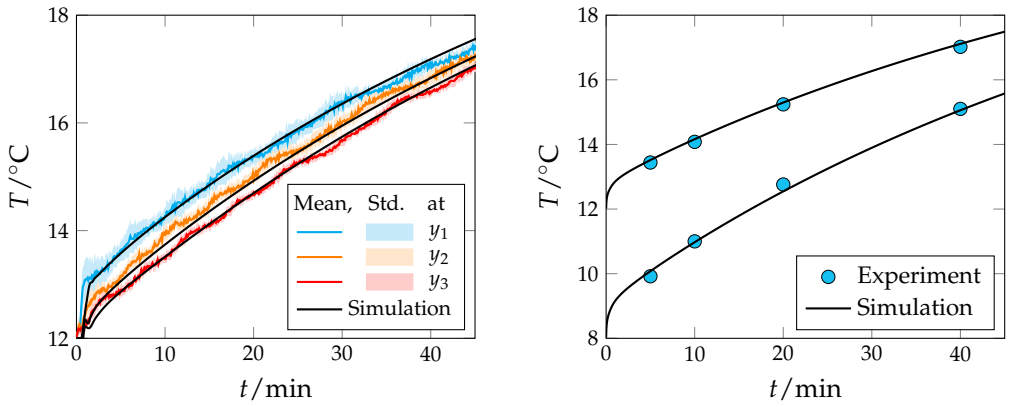

Figure 6. Validating the simulation for water warming at $T_R = 23\,^{\circ}\mathrm{C}$ with the temperature at three positions (y_1, y_2, and y_3) in the water ($T_0 = 12\,^{\circ}\mathrm{C}$) and the average water temperature for $T_0 = 8\,^{\circ}\mathrm{C}$ and $T_0 = 12\,^{\circ}\mathrm{C}$. (**a**) Temperature at three positions. (**b**) Average temperature.

Figure 7 shows the resulting average water temperatures compared to the experimental data. The baseline simulation computes the temperature only 0.09 °C higher than the experiment at $t = 40\,\mathrm{min}$. Leaving out one of the mechanisms reduces the temperature increase over time. The convection of water affects the warming the least, whereas the convection of the air has a more significant influence. Without considering the water convection, the temperature increase after 40 min is 0.3 °C lower compared to the experiment. This corresponds to a relative error of 6.0% in relation to the absolute temperature change. For the air convection, the error is 19.7% or 1.0 °C. Surprisingly, radiation has a relatively large influence and affects warming more than convection. Not including radiation in the simulation results in a 1.7 °C lower temperature, corresponding to a relative error of 33.6%. This is unexpected, since most practitioners probably consider the influence of radiation negligible at relatively low present temperatures. However, the result is well in agreement with the standard literature, compared to example 16.5-2 in [37], which features comparable absolute temperatures, temperature differences, and emissivities. Without simulating radiation and convection of the room air, the predicted temperature is off by 66.3% or 3.3 °C. These results show that the numerical simulation has to account for the convection and, especially, the radiation to appropriately model the heat transfer for liquid warming in a glass. A simple heat transfer model considering only the heat conduction would not be sufficient to depict the complex physical process. The local and temporal effects of the physical heating mechanisms are discussed more closely in Section 5.

Now, the simulation for red wine warming in the glass was evaluated with the average wine temperature in Figure 8a. The simulation agrees very closely with the experiment, as before for water. The difference after 40 min is only 0.07 °C for both initial temperatures, which corresponds to a relative error of 1.4% or 1.0%, respectively. The largest error is only 0.18 °C, or 2.6%, for $T_0 = 8\,^{\circ}\mathrm{C}$ after 20 min.

Figure 8b compares the simulation results for water and wine. Hardly any difference in the average temperature can be observed. The temperature after 40 min differs only by 0.07 °C for both initial temperatures. The experimental data support the simulation results since the temperature for water and wine were also nearly the same in the experiments. The comparison of the material properties of the examined water and aqueous ethanol solution at 20 °C yields a deviation of about 0.9% for the density, 2.2% for the specific

heat capacity, and 11.5% for the heat conductivity. The investigated wine has a relatively high alcohol content of 13.5%. Since wine usually does not exceed 15.0%, no significant deviating simulation results are expected for other wines. For wines with lower alcohol content, the temperature difference between the wine and water simulation is even more negligible. Consequently, one can assume that deviating fluid properties of wine due to the alcohol content do not significantly affect the heat transfer. Simulation results are therefore valid for all types of non-sparkling wine with negligible or moderate sugar levels. The possible impact of the sugar content was already discussed in Section 2.2. Furthermore, it would be sufficient to model wine as water. The simulation approach can be applied to comparable non-sparkling beverages with similar properties. In conclusion, the presented simulation accurately represents the warming process of wine in a glass only when considering convection and radiation.

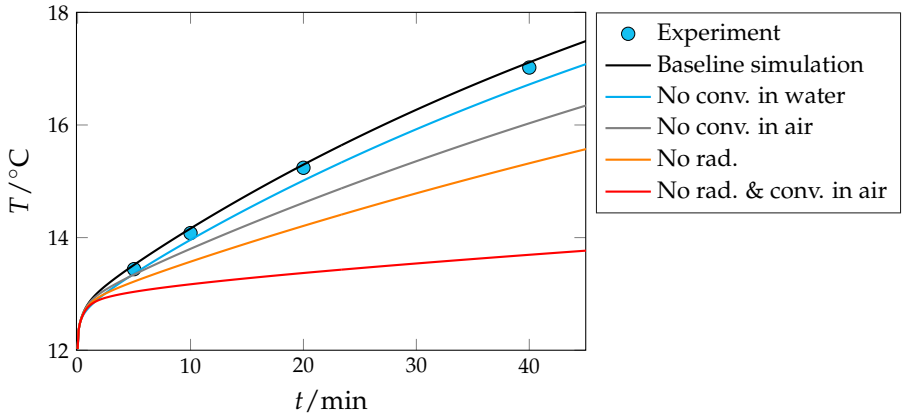

Figure 7. Impact of neglecting convection (conv.) and radiation (rad.) in the simulation for warming water at $T_R = 23\,°C$.

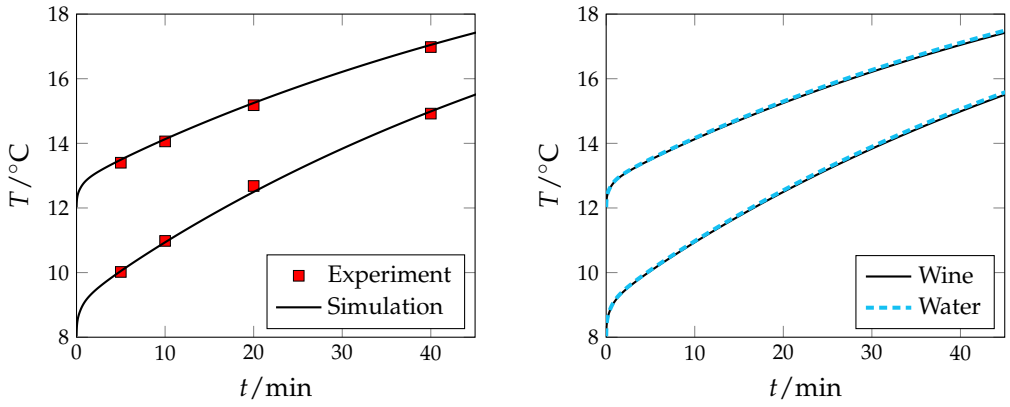

(**a**) (**b**)

Figure 8. Validating the simulation with the average temperature of red wine warming at $T_R = 23\,°C$ and the comparison to the corresponding simulation for water for $T_0 = 8\,°C$ and $T_0 = 12\,°C$. (**a**) Red wine average temperature. (**b**) Simulation of red wine and water.

5. Results and Discussion

The validated simulation model was now applied to closely investigate wine warming in the glass. Analyzing the simulation results answers a few fundamental questions. For example, which heating mechanisms dominate, and where do they act? Or, how does the heat intake in wine evolve temporally and locally? The investigation considers the warming of wine with the initial temperature $T_0 = 12\,°C$ at room temperature $T_R = 23\,°C$. Red wine is used in the simulation, but Section 4 shows that the results apply to many types of non-sparkling wine, excluding sweet wines with high sugar content. Furthermore,

a parameter study presents the wine's temperature increase over time for various combinations of the initial wine and room temperature. The results show how quickly wine warms up under different temperature conditions. Examples are given of how to use these insights in practice. All investigations apply the simulation model, presented in Section 3, for the problem configuration described in Section 2.

5.1. Governing Physical Heating Mechanisms of the Warming Process

Initially, the (sensible) heat of the glass is transferred to the wine by conduction. Buoyant flow starts to form. It is characterized by warmer wine with a lower density that rises in the wall area towards the surface. Accelerated fluid velocities lead to increased heat transfer from glass to wine, as cold wine is directed toward the glass. It should be noted that the convective heat transfer includes the conductive contribution, as the two cannot be subdivided at the boundary. The maximum velocity magnitude of the natural convective flow is $2.4 \times 10^{-3}\,\mathrm{m\,s^{-1}}$, which occurs within the first minute of the observation in the vicinity of the wall. The average velocity magnitude in wine peaks at $8.23 \times 10^{-4}\,\mathrm{m\,s^{-1}}$; see Figure 9b. Warmer liquid rises in the wall area, passes by the surface towards the center, and then returns downwards to the stem wall along positions y_1 to y_3; see Figure 9a. When the fluid reaches the lower part of the glass, one can observe a slight increase in velocities due to the narrowing of the glass; see $t = 120$ s in Figure 9b, for example.

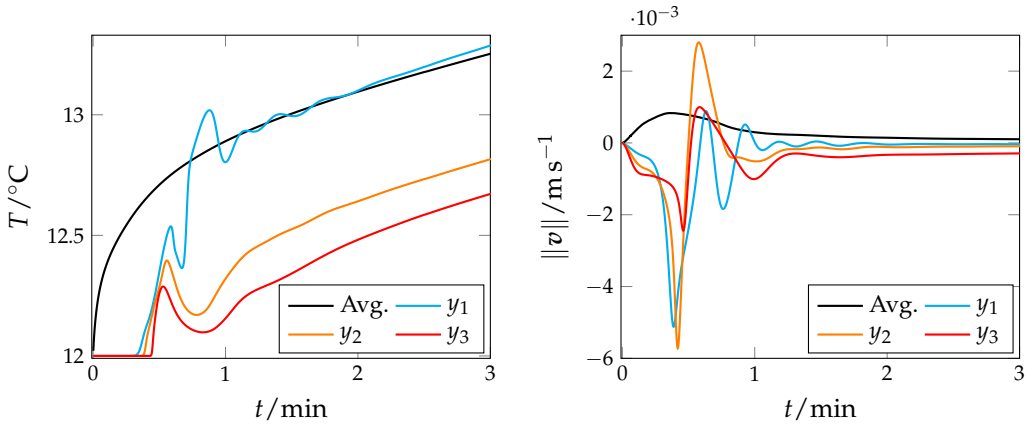

(**a**) Temperature (**b**) Velocities

Figure 9. Decline of buoyant effects after one minute for temperatures and velocities. Probes at positions on the symmetry axis and volumetric averages.

The uptake of sensible heat from glass walls and initial natural convection result in the accelerated warming of wine within the first minute; see Figure 9a. The magnitude of the velocities remains comparably moderate after the initial shocks within the first minute; see Figures 9b and 10. The Reynolds number in the liquid domain ($H = 127\,\mathrm{mm}$) is $Re = \max(\|\boldsymbol{v}\|)\, H/\nu \approx 260$, where ν is the kinematic viscosity. The maximum Grashof number is $Gr = g_1\, \beta\, (T_\mathrm{W} - T_0) H^3/\nu \approx 4.38 \times 10^6$, where the index W denotes the glass wall temperature, and β is the thermal expansion coefficient. The Grashof number relates viscous forces to natural convective forces and helps to decide whether a turbulent buoyancy is to be expected. Turbulent boundary layers are present for $Gr > 4 \times 10^8$ [38], which is two orders of magnitude higher than the maximum Grashof number within this work. The assumption of laminar flow in the liquid domain is, hence, valid. Investigating the natural convection closer, it does not seem to be able to equilibrate the temperature in wine. One can observe a stratification in temperatures from two minutes onwards; see Figure 11. This finding aligns with the findings from the model validation, where the exclusion of wine convection did not alter the simulation outcome considerably.

As the wine starts to cool the wine glass, the latter engages in net radiative heat exchange with surrounding warmer walls of the air domain. The validation in Figure 7

demonstrates the dominant influence of radiation. Moreover, the temperature difference enables sensible heat transfer from the air at room temperature into the glass; see Figure 11. Due to the higher density of cooler air, the air starts to fall past the glass and then hovers horizontally away on the table; see Figure 12. A natural convection cell forms in the air domain. The cooled air tumbles through the problem domain and regains room temperature before it may again pass by the glass. Figure 11 underlines that air continuously approaches the glass at room temperature. After one hour, the approaching air still has $T_{\mathrm{air}} = 22.997\,^{\circ}\mathrm{C}$, which confirms that the natural convection of air in a room can be modeled in a closed cavity with constant wall temperatures. The maximum velocity in the vicinity of the glass is $1.4 \times 10^{-1}\,\mathrm{m\,s^{-1}}$. The corresponding Reynolds number ($H = 225\,\mathrm{mm}$) is $Re \approx 2000$ and Grashof number is $Gr \approx 2.44 \times 10^{7}$. Hence, the initial assumption of dominantly laminar airflow seems valid for the scope of this work.

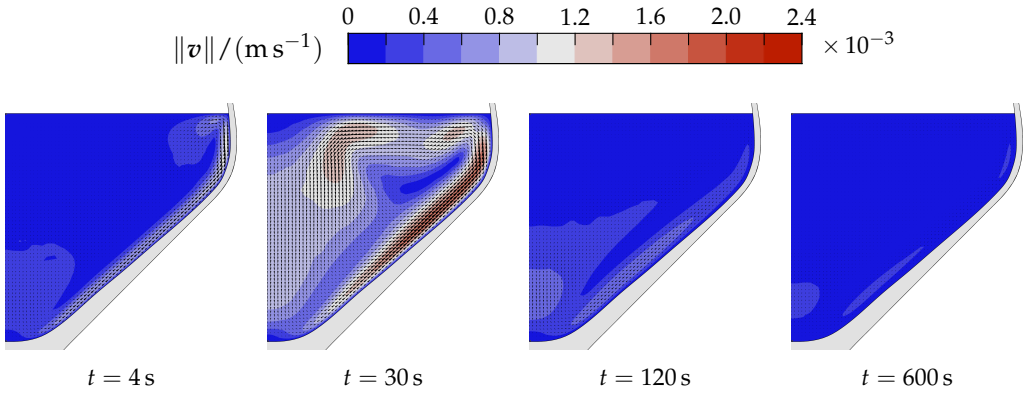

Figure 10. Velocity distribution in the wine for $T_0 = 12\,^{\circ}\mathrm{C}$ and $T_{\mathrm{R}} = 23\,^{\circ}\mathrm{C}$ in the symmetry plane.

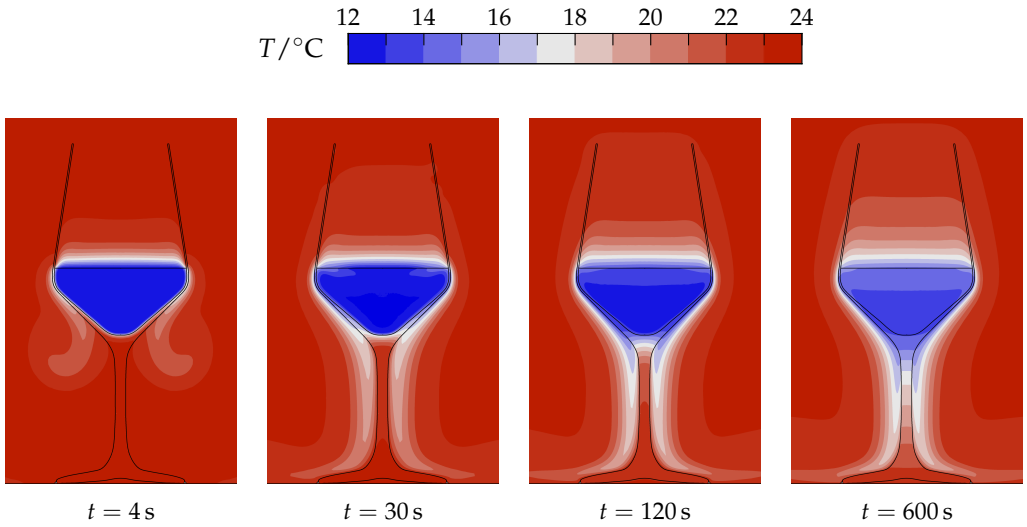

Figure 11. Temperature distribution in the wine, air, and glass for $T_0 = 12\,^{\circ}\mathrm{C}$ and $T_{\mathrm{R}} = 23\,^{\circ}\mathrm{C}$ in the symmetry plane.

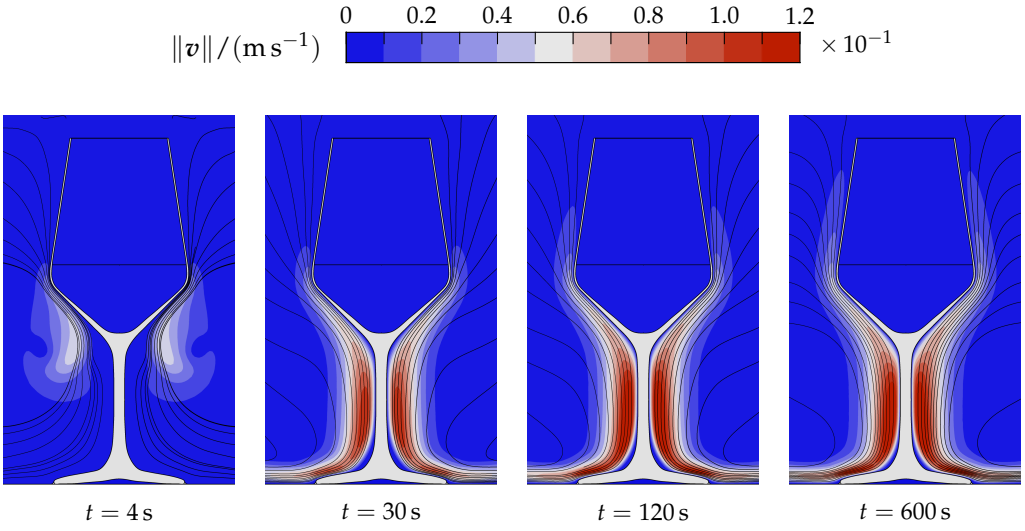

Figure 12. Velocity distribution in the air and wine for $T_0 = 12\,^{\circ}\mathrm{C}$ and $T_R = 23\,^{\circ}\mathrm{C}$ in the symmetry plane.

5.2. Spatial and Temporal Heat Flux Analysis

After describing the physical heating effects during the warming process, this section provides answers concerning where and when these effects occur. Figure 13a,b depict the heat intake Q from the surrounding air domain. At the liquid surface, convective and radiative heat fluxes add up to the total heat intake. The dominance of radiative heat flux and the overall low magnitude of heat transfer by convection can be explained by a stagnation of the natural convective airflow in the opening of the glass; see Figure 12. Consequently, a pronounced thermal boundary layer can build up; see Figure 11. The reduced air temperature trapped in the glass leads to a reduced driving temperature difference for heat conduction at the surface. At the glass–air interface, heat fluxes start to form with continuously decreasing glass temperatures, as, initially, the glass and air both are at T_R. Radiative and convective heat fluxes at the air–glass interface do not add up to the total heat flux that enters the wine; see Figure 13b. The difference results from the sensible heat of the glass, which is transferred predominantly within the first minutes of the simulation. The magnitude of heat intake at the glass–wine interface is up to two orders larger than at the air–wine interface. Radiation, again, slightly dominates the heat intake into the glass, which is also reflected in the model validation; see Figure 7. All in all, the main heat stems from the outside convection of air and the radiative heat exchange of the glass with surrounding walls and the table. The maximum conductive heat flux from the table is $1.2 \times 10^{-2}\,\mathrm{W}$ and, hence, can be neglected. Both radiative and convective heat transfers govern the second warming period for $t > 2\,\mathrm{min}$, when the sensible heat exchange of the glass diminishes. Radiative and convective fluxes reach their maximum after approximately ten minutes. Afterwards, the mechanisms again gradually attenuate as the driving temperature difference between glass and room temperature decreases.

To analyze the local effects of heat transfer, the heat flux at the wine–glass interface ($\mathrm{W\,m^{-2}}$) is integrated over horizontal lines of equal heights, such that one can evaluate the integrated heat flux ($\mathrm{W\,m^{-1}}$) at variable y-positions. Figure 14a illustrates these height-dependent heat fluxes at the interface at discrete points in time. Although a dominant heat flux from the stem could be expected, this is not the case. Dominant heating comes from the thin parts of the glass at elevated heights. The heat flux attenuates by one order of magnitude within the first two minutes, where the exchange of sensible heat of the glass dominates the heating. The heat flux from air to the outer wine glass surface at $t = 10\,\mathrm{min}$ is analyzed in Figure 14b. The dominant convective heat flux appears in a small vertical zone of the glass $y \in [125, 150]\,\mathrm{mm}$, where the glass diameter is large. Below this area, the airflow slightly detaches from the glass, which leads to decreased convective heat

flux. In the stem and foot area, the cold air regains heat from the glass. On the contrary, the radiative heat exchange can occur within the full range of heights where wine is located on the other side of the wall.

Overall, one can differentiate between two heating periods. Within the first minutes, accelerated heating takes place. The driving mechanisms are the transfer of sensible heat from the glass to the wine and subsequent natural convection. The second period is characterized by the radiative and convective heating of the wine glass that occurs at the outer surface of the glass.

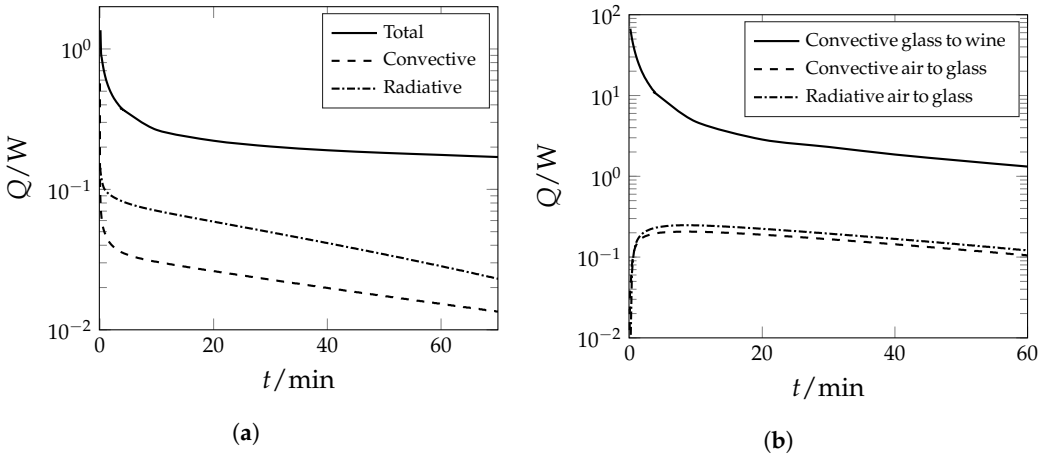

(**a**) (**b**)

Figure 13. Temporal analysis of convective and radiative heat fluxes. (**a**) Heat fluxes at the air–wine interface over time. (**b**) Heat fluxes at glass–wine and glass–air interfaces over time.

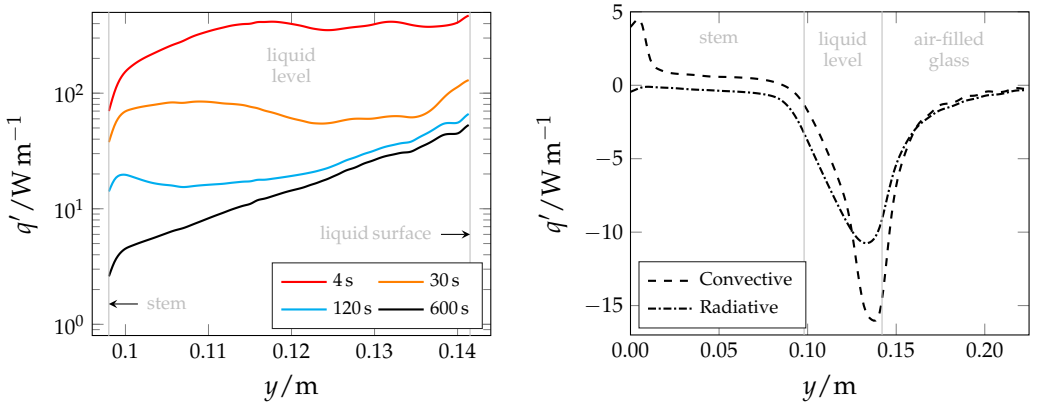

(**a**) (**b**)

Figure 14. Spatial analysis of convective and radiative heat fluxes. (**a**) Inner wall of glass: heat flux to wine integrated over y = const. isolines. (**b**) Outer wall of the glass. Heat fluxes at $t = 600\,\mathrm{s}$ integrated over y = const. isolines.

5.3. Temperature Study

After revealing the underlying physical heating phenomena, a parameter study for various combinations of the initial wine and the room temperature was performed. The study included the temperature conditions of $T_0 \in \{6, 8, 10, 12, 14\}\,^\circ\mathrm{C}$ and $T_\mathrm{R} \in \{20, 23, 26, 29\}\,^\circ\mathrm{C}$. The warming is discussed more closely for $T_\mathrm{R} = 23\,^\circ\mathrm{C}$ and $T_\mathrm{R} = 29\,^\circ\mathrm{C}$, which resemble a common room temperature and the temperature on a hot summer day, respectively.

Figure 15 presents the increase of the average wine temperature over time for all combinations. As expected, the temperature rises quicker for higher room temperatures and lower initial temperatures. The previously identified two heating periods primarily determine the temperature development. The initial rapid temperature change due to the intake of the glass' sensible heat is followed by a moderate, almost constant temperature

increase driven by convection and radiation. The rapid warming occurs during the first 2 to 3 min for all conditions. The temperature change over the first minute is about 0.6 °C to 1.2 °C for 23 °C and 1.2 °C to 1.7 °C for 29 °C room temperature. The rate of change is about 0.1 °C/min to 0.2 °C/min at $T_R = 23$ °C and 0.2 °C/min to 0.3 °C/min at $T_R = 29$ °C after a few minutes.

The following examples are potential practical conclusions drawn from Figure 15. On a summer day with $T_R = 29$ °C, a white wine warms up from 8 °C to 11 °C in only 5 min. The wine is warmer than 12 °C after 10 min. Hence, it could be beneficial to reduce the storage temperature at a restaurant or bar to serve the white wine not too warm, considering the time of serving. The glasses could also be cooled in advance to reduce the initial heat transfer from the glass. At the same ambient temperature, red wine poured at 12 °C reaches 15 °C after only 8 min. Consequently, it could be desirable to keep red wine relatively cool rather than serving it too warm owing to storage at room temperature. Another scenario could be having a glass of red wine for a nice dinner at home at a room temperature of 23 °C: If the red wine was stored in a cellar or refrigerator at 12 °C, it warms up to 15 °C to 16 °C after 18 to 27 min. This period could be ideal for aerating the wine in the glass until it reaches optimal drinking temperature while finishing the dinner preparation.

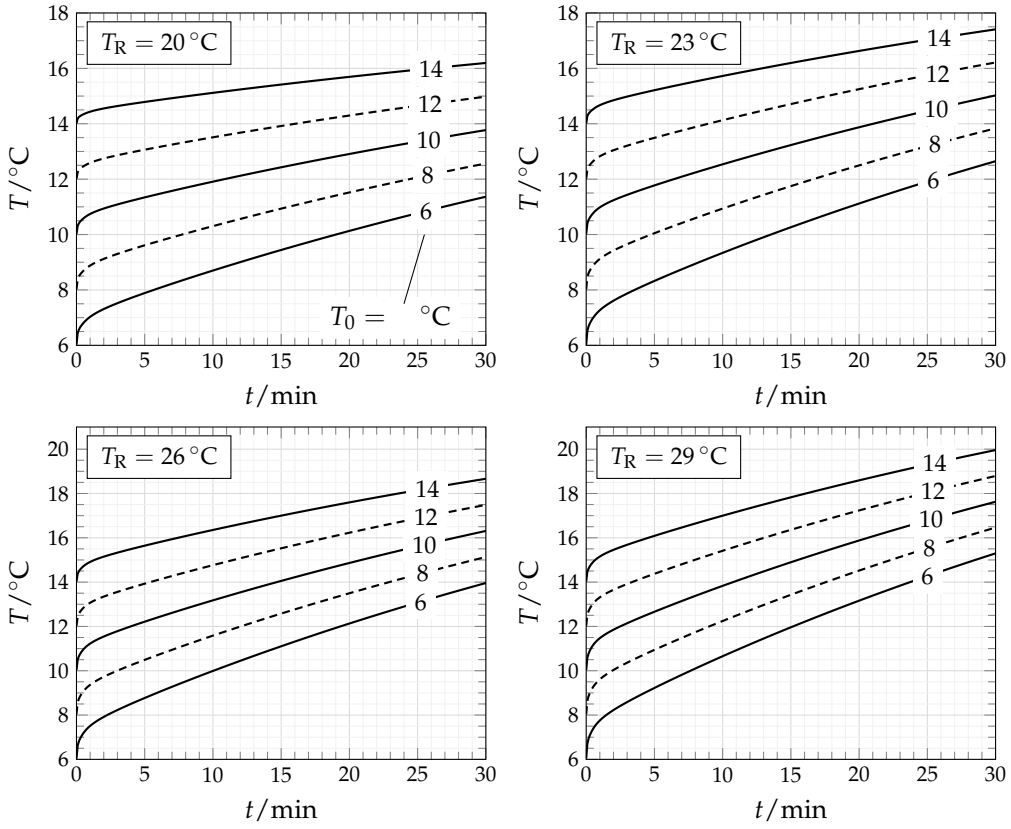

Figure 15. Temperature increase over time of 150 mL of wine in a wine glass depending on the room temperature T_R and initial wine temperature T_0.

6. Conclusions

This study investigated the warming of wine since the temperature significantly affects the wine's sensory attributes. It provides the physical knowledge to obtain the desired drinking temperature. The presented simulation approach accurately represents the physical process of wine warming in a glass, as validated by experiments with excellent agreement. The simulation must account for heat conduction, convection, and even thermal radiation to model the heat transfer appropriately. Leaving out thermal radiation or natural air convection leads to highly inaccurate results with relative errors of up to 66.3%. The most convective and radiative heat is introduced into the wine at a narrow horizontal

band at the outer wall, where the glass diameter is maximal. Accelerated initial heating is governed by natural convection in wine due to the uptake of the sensible heat of the glass. Simulations and experiments suggest that the influence of the alcohol content can be neglected concerning wine warming. Therefore, the results apply to all non-sparkling wines with moderate sugar content for the investigated configuration.

For 150 mL of wine in a medium-sized red wine glass, the temperature increase over time was determined for various combinations of initial wine (storage) and surrounding (room) temperatures. The results can give insight into how to prepare wine in varying ambient climates. The parameter study for arbitrary storage and room temperature configurations should be extended to different filling quantities, glass shapes, and wall thicknesses to obtain broader information on the temperature increase. Future studies could also consider warming wine in a decanter, which is commonly used to aerate wines for a relatively long period. In the future, a framework recently published by the authors [39,40] will be used to derive fast and accurate metamodels, so-called digital twins, from the CFD data. The predicted warming time to reach the optimal drinking temperature could then be provided in the form of a lean app that is easily accessible to sommeliers, restaurateurs, and wine lovers.

Author Contributions: Conceptualization, M.K. and F.K.; data curation, M.K. and F.K.; formal analysis, M.K. and F.K.; investigation, M.K. and F.K.; methodology, M.K. and F.K.; project administration, M.S.; resources, M.S.; software, M.K. and F.K.; supervision, M.S.; validation, M.K. and F.K.; visualization, M.K. and F.K.; writing—original draft, M.K. and F.K.; writing—review and editing, M.K. and F.K. All authors have read and agreed to the published version of the manuscript.

Funding: The APC was funded by the Open Access Publishing Fund of Technical University of Darmstadt.

Institutional Review Board Statement: Not applicable.

Informed Consent Statement: Not applicable.

Data Availability Statement: The original contributions presented in the study are included in the article, further inquiries can be directed to the corresponding author.

Acknowledgments: The authors would like to thank Stölzle Lausitz GmbH (Weißwasser/Oberlausitz, Germany) for providing the dimensions and material properties of their wine glass. Moreover, the authors would like to acknowledge Christian Dietz for giving valuable insights into the serving of wine from a sommelier's perspective. The work of Maximilian Kannapinn is supported by the Graduate School CE within the Centre for Computational Engineering at Technical University of Darmstadt.

Conflicts of Interest: The authors declare no conflicts of interest.

References

1. Ross, C.F.; Weller, K. Effect of serving temperature on the sensory attributes of red and white wines. *J. Sens. Stud.* **2008**, *23*, 398–416. [CrossRef]
2. Robinson, J.; Harding, J. *The Oxford Companion to Wine*; American Chemical Society: Washington, DC, USA, 2015.
3. Beaumont, F.; Liger-Belair, G.; Polidori, G. Computational Fluid Dynamics (CFD) as a tool for investigating self-organized ascending bubble-driven flow patterns in champagne glasses. *Foods* **2020**, *9*, 972. [CrossRef] [PubMed]
4. Beaumont, F.; Popa, C.; Liger-Belair, G.; Polidori, G. Temperature dependence of ascending bubble-driven flow patterns found in champagne glasses as determined through numerical modeling. *Adv. Mech. Eng.* **2013**, *5*, 156430. [CrossRef]
5. Bogard, F.; Beaumont, F.; Vasserot, Y.; Simescu-Lazar, F.; Nsom, B.; Liger-Belair, G.; Polidori, G. Combined experimental and CFD approach of two-phase flow driven by low thermal gradients in wine tanks: Application to light lees resuspension. *Foods* **2020**, *9*, 865. [CrossRef] [PubMed]
6. Schmidt, D.; Velten, K. Modeling and simulation of the bubble-induced flow in wine fermentation vessels. In Proceedings of the BIO Web of Conferences, EDP Sciences, Mainz, Germany, 5–10 July 2015; Volume 5, p. 02015. [CrossRef]
7. Schmidt, D.; Velten, K. Numerical simulation of bubble flow homogenization in industrial scale wine fermentations. *Food Bioprod. Process.* **2016**, *100*, 102–117. [CrossRef]

8. Söylemez, E.; Alpman, E.; Onat, A.; Hartomacıoğlu, S. CFD analysis for predicting cooling time of a domestic refrigerator with thermoelectric cooling system. *Int. J. Refrig.* **2021**, *123*, 138–149. [CrossRef]
9. Hopfgartner, J.; Heimel, M.; Posch, S.; Berger, E.; Almbauer, R.; Schlemmer, S. Numerical simulation of the 3D transient temperature evolution inside a domestic single zone wine storage cabinet with forced air circulation. In Proceedings of the 16th International Refrigeration and Air Conditioning Conference, West Lafayette, IN, USA, 11–14 July 2016.
10. Santolini, E.; Barbaresi, A.; Torreggiani, D.; Tassinari, P. Numerical simulations for the optimisation of ventilation system designed for wine cellars. *J. Agric. Eng.* **2019**, *50*, 180–190. [CrossRef]
11. Košmerl, T.; Abramovič, H.; Klofutar, C. The rheological properties of slovenian wines. *J. Food Eng.* **2000**, *46*, 165–171. [CrossRef]
12. Travnicek, P.; Burg, P.; Krakowiak-Bal, A.; Junga, P.; Vitez, T.; Ziemianczyk, U. Study of rheological behaviour of wines. *Int. Agrophys.* **2016**, *30*, 509–518. [CrossRef]
13. Hlaváč, P.; Božiková, M.; Hlaváxcxová, Z.; Kubík, L. Influence of temperature and storing time on selected red wine physical properties. *Acta Univ. Agric. Silvic. Mendel. Brun.* **2016**, *64*, 433–439. [CrossRef]
14. Green, B.G.; Frankmann, S.P. The effect of cooling on the perception of carbohydrate and intensive sweeteners. *Physiol. Behav.* **1988**, *43*, 515–519. [CrossRef]
15. Jackson, R.S. *Wine Tasting: A Professional Handbook*; Academic Press: Cambridge, MA, USA, 2016.
16. Ross, C.F.; Weller, K.M.; Alldredge, J.R. Impact of serving temperature on sensory properties of red wine as evaluated using projective mapping by a trained panel. *J. Sens. Stud.* **2012**, *27*, 463–470. [CrossRef]
17. Arakawa, T.; Iitani, K.; Wang, X.; Kajiro, T.; Toma, K.; Yano, K.; Mitsubayashi, K. A sniffer-camera for imaging of ethanol vaporization from wine: The effect of wine glass shape. *Analyst* **2015**, *140*, 2881–2886. [CrossRef] [PubMed]
18. Tucker, G.; Hanby, E.; Brown, H. Development and application of a new time–temperature integrator for the measurement of *p*-values in mild pasteurisation processes. *Food Bioprod. Process.* **2009**, *87*, 23–33. [CrossRef]
19. Wolny-Koładka, K.; Malinowski, M.; Zdaniewicz, M. Energy-related and microbiological evaluation of the effects of bulking agents on the brewery hot trub biodrying. *Food Bioprod. Process.* **2021**, *127*, 398–407. [CrossRef]
20. Luna, R.; Matias-Guiu, P.; López, F.; Pérez-Correa, J.R. Quality aroma improvement of muscat wine spirits: A new approach using first-principles model-based design and multi-objective dynamic optimisation through multi-variable analysis techniques. *Food Bioprod. Process.* **2019**, *115*, 208–222. [CrossRef]
21. Soleas, G.J.; Diamandis, E.P.; Goldberg, D.M. Wine as a biological fluid: History, production, and role in disease prevention. *J. Clin. Lab. Anal.* **1997**, *11*, 287–313. [CrossRef]
22. Bird, R.B.; Stewart, W.E.; Lightfoot, E.N. *Transport Phenomena*, 2nd ed.; Wiley: Hoboken, NJ, USA, 2007.
23. ANSYS, Inc. ANSYS CFX-Solver Theory Guide—Release 2021 R1. Available online: https://www.ansys.com/ (accessed on 8 November 2023).
24. Incropera, F.P.; DeWitt, D.P.; Bergman, T.L.; Lavine, A.S. *Fundamentals of Heat and Mass Transfer*, 6th ed.; Wiley: Hoboken, NJ, USA, 2006.
25. Shah, N.G. New Method of Computation Heat Transfer in Combustion Chambers. Ph.D. Thesis, University of London, London, UK, 1979.
26. Melinder, Å. Thermophysical Properties of Aqueous Solutions Used as Secondary Working Fluids. Ph.D. Thesis, KTH Stockholm, Stockholm, Sweden, 2007.
27. Verein Deutscher Ingenieure. *VDI Wärmeatlas*; Springer: Berlin/Heidelberg, Germany, 2006. [CrossRef]
28. Baehr, H.D.; Stephan, K. *Heat and Mass Transfer*, 3rd ed.; Springer: Berlin/Heidelberg, Germany, 2011.
29. Brewster, M.Q. *Thermal Radiative Transfer and Properties*; John Wiley & Sons: Hoboken, NJ, USA, 1992.
30. Tsilingiris, P. Thermophysical and transport properties of humid air at temperature range between 0 and 100 °C. *Energy Convers. Manag.* **2008**, *49*, 1098–1110. [CrossRef]
31. Rubin, M. Optical properties of soda lime silica glasses. *Sol. Energy Mater.* **1985**, *12*, 275–288. [CrossRef]
32. Radmanović, K.; Dukić, I.; Pervan, S. Specific heat capacity of wood. *Wood Ind. Ind.* **2014**, *65*. [CrossRef]
33. Niemz, P. Untersuchungen zur Wärmeleitfähigkeit ausgewählter einheimischer und fremdländischer Holzarten. *Bauphysik* **2007**, *29*, 311–312. [CrossRef]
34. Rice, R.W. Emittance factors for infrared thermometers used for wood products. *Wood Fiber Sci.* **2004**, *36*, 520–526.
35. Scheid, M. Thermodynamische und Strukturmechanische Untersuchungen von auf Kontakthitze Basierenden Gartechnik-Komponenten Mittels Finite-Element-Methoden und Numerischer Strömungssimulation. Master's Thesis, Technische Universität Darmstadt, Darmstadt, Germany, 2017.
36. Roache, P.J. Perspective: A method for uniform reporting of grid refinement studies. *J. Fluids Eng.* **1994**, *116*, 405–413. [CrossRef]
37. Bird, R.B.; Steward, W.E.; Lightfoot, E.N.; Klingenberg, D.J. *Introductory Transport Phenomena*, 1st ed.; Wiley: Hoboken, NJ, USA, 2015.
38. Smith, R.; Inomata, H.; Peters, C. Heat transfer and finite-difference methods. In *Introduction to Supercritical Fluids*; Smith, R., Inomata, H., Peters, C., Eds.; Supercritical Fluid Science and Technology; Elsevier: Amsterdam, The Netherlands, 2013; Volume 4, pp. 557–615. [CrossRef]

39. Kannapinn, M.; Pham, M.K.; Schäfer, M. Physics-based digital twins for autonomous thermal food processing: Efficient, non-intrusive reduced-order modeling. *Innov. Food Sci. Emerg. Technol.* **2022**, *81*, 103143. [CrossRef]
40. Kannapinn, M.; Schäfer, M.; Weeger, O. Twinlab: A framework for data-efficient training of non-intrusive reduced-order models for digital twins. *Eng. Comput.* **2024**. [CrossRef]